32nd Annual International Conference of the IEEE EMBS
Buenos Aires, Argentina, August 31 - September 4, 2010

On the Controllability of Dynamic Model-Based Needle Insertion in Soft Tissue

Amir Haddadi[†] , Orcun Goksel[‡], Septimiu E. Salcudean[‡], and Keyvan Hashtrudi-Zaad[†]

Abstract— **Soft tissue needle guidance and steering for clinical applications has been an active topic of research in the past decade. Although dynamic feedback control of needle insertion systems is expected to provide more accurate target tracking, it has received little attention due to the fact that most available models for needle-tissue interaction do not incorporate the dynamics of motions. In this paper, we study the controllability of rigid or flexible needles inside soft tissues using mechanical-based dynamic models. The results have significant implications on the design of suitable feedback controllers for different types of needle insertion systems.**

I. INTRODUCTION

Needle and catheter insertion is a common step taken in many clinical diagnostic and therapeutic procedures. Such procedures include tissue biopsy [1], radioactive seed implantation in brachytherapy [2], and anesthetic insertion [3]. In order to minimize damage to the patient body, needles are normally flexible, long and slender, which causes needle deflections during needle insertion procedures. Also inserting and retracting needles cause soft tissues to deform. In addition to the above factors, tissue swelling and deformation due to edema and tissue movements due to respiration influence the accuracy with which the needle can be guided to a desired target inside the soft tissue [4], [5].

Robot-assisted needle insertion has recently received significant attention for its potential capability in delivering highly accurate targeting [1], [3], [6], [7]. Due to the lack of an accurate yet simple enough dynamic model for the coupled needle-tissue system [8], most of the related studies are focused on computer simulations [9], [10], pre-planning [4], steering [11], and path-planning [12], rather than the automatic control of the flexible needle.

Path-planning, by itself, is not sufficient to proceed to robot-assisted needle insertion, unless there is a control system which can control the needle to track the designed path. Pre-planning is an offline process in which the needle insertion parameters such as the insertion angle and bevel orientation are derived prior to the insertion [4]. Steering is a closer approach to a control strategy. DiMaio *et al.* [11] derived a needle manipulation Jacobian, which relates the desired needle tip to base velocities, using numerical needle insertion models that includes needle deflection and tissue deformation. Glozman *et al.* [6] used the analytical forward and inverse kinematics of a simplified needle-tissue model to determine the required needle base trajectory for any desired needle tip trajectory. Although real-time, the steering methods do not compensate for unwanted errors and disturbances applied to the needle tip, as opposed to closed-loop control of the base. Thus, there is a need to design appropriate control methodologies for flexible needle insertion [3].

Studies on feedback control of needle insertion are very limited [3]. Hauser *et al.* proposed a closed-loop model predictive controller that would steer the needle along helical paths to reach a desired target position based on a kinematic model of the circular movements of the needle caused by the bevel tip [13]. For such models there is no distinct relation between input forces and control objective or tip position, which requires needle dynamic equations. Reed *et al.* control bevel-tip orientation through a torque applied about the needle base in the presence of torsional friction [14]. They use a dynamic model of the needle inside the soft tissue as a continuum medium and design their controller. In such cases, as in all dynamic control methods, a question remains to be answered is whether or not the proposed dynamic models are controllable.

In this paper, we will first derive a dynamic model for a rigid needle inside a soft tissue modeled by the finite element method. We will determine the nonlinear controllability of the system states in the entire operational workspace. We will then incorporate the angular-spring method [15] in a mechanical-based dynamic model of the flexible needle and will discuss system controllability of the nonlinear and linearized models. The results will lead to some important conclusions regarding feedback control of rigid and flexible needles inside soft tissues.

II. CONTROL OF RIGID NEEDLES IN SOFT TISSUE

In this section, we will analytically derive a dynamic model of a rigid needle moving inside a soft tissue in a two-dimensional plane (2D), as illustrated in Figure 1. We will investigate whether the needle-tip can be controlled to reach any desired path, while avoiding obstacles in the 2D plane. The control actuation is provided by the input force F_{in} along the needle base and the input torque τ_{in} about the axis perpendicular to the plane of motion. The tissue dynamics is modeled by a finite element model (FEM). In order to model the tissue-needle interaction forces using the FEM, we consider a number of nodes (in this case three) along the needle as shown with dark (red) circles. Each node separates one link from the next one. The mass and the length of each link are denoted by m and L. Without

[†] Department of Electrical and Computer Engineering, Queen's University, Kingston, ON K7L 3N6, Canada. email: khz@post.queensu.ca.
[‡] Department of Electrical and Computer Engineering, The University of British Columbia, Vancouver, BC, Canada.

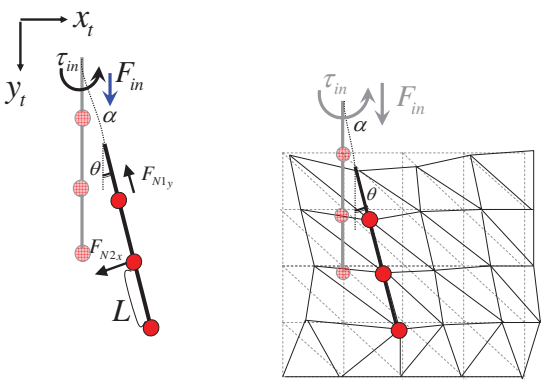

Fig. 1. Model of the rigid needle and the interaction forces.

loss of generality, the examples of this paper are presented for a 3-segment needle model.

A. Dynamic model of rigid needles

We use the energy-based Lagrange approach [16] to reach the dynamics of the coupled system. Our method considers the needle-tissue interaction forces as external forces and requires kinetic and potential energy of the needle. If we consider the mass of each link at its distal end, and assume that the needle moves $\delta\alpha$ in the direction of the needle and rotates $\delta\theta$ about the axis perpendicular to the plane, the displacement of the mass of each link $(\delta x_{mi}, \delta y_{mi})$ represented in the fixed Cartesian coordinates, shown by x_t and y_t in Figure 1, is calculated as

$$\delta x_{mi} = \delta\alpha sin\theta + iL\delta\theta cos\theta, \quad \delta y_{mi} = \delta\alpha cos\theta - iL\delta\theta sin\theta$$

where $i = 1, 2, 3$ is the link number. These small displacements can be used to derive velocities of each link along x_t and y_t directions. As a result, the kinetic energy of the needle is calculated as

$$\mathcal{K}_n = \frac{1}{2}\sum_{i=1}^{3} m(\dot{\alpha}^2 + i^2L^2\dot{\theta}^2) \; + \; \frac{3}{2}I\dot{\theta}^2 \tag{1}$$

where I is the link's moment of inertia. The potential energy of the rigid needle is zero.

We consider the effect of needle-tissue interaction as external forces acting perpendicular to and along the needle at the three nodes, *i.e.* $\mathbf{F_{Ni}} = [F_{Ni_x}\, F_{Ni_y}]$, on the coordinate attached to the needle, as shown in Figure 1. Using Lagrange's approach, the dynamic equations of the coupled system for the rigid needle can be derived as

$$\ddot{\alpha}(3m) = F_{in} - \sum_{i=1}^{3} F_{Niy} - F_f \tag{2}$$

$$\ddot{\theta}(14mL^2 + 3I) = \tau_{in} - L\sum_{i=1}^{3} iF_{Nix}. \tag{3}$$

where α represents net translation of the needle, which is found as a sum of the needle linear displacements in the direction of its base link at each instant of time. The forces F_{Niy} are chosen based on the stick or slip modes of the needle-tissue interaction model [17]. The force $F_f = B_f\dot{\alpha}$ is the friction force along the needle shaft, and the forces F_{Nix} and F_{Niy} are achieved from the FEM of the tissue.

To derive the tissue-needle interaction forces, we consider the interaction nodes of the tissue with the needle as the *working* nodes and the rest of the tissue nodes as the *non-working* nodes. If we denote the external forces and displacements of the working and non-working nodes as $\mathbf{F_w}$, $\mathbf{F_{nw}}$, $\mathbf{u_w}$, and $\mathbf{u_{nw}}$, respectively, and consider the tissue as an elastic object, then the forces at each node, are directly related to the movement of each FEM node according to [17]

$$\begin{pmatrix} \mathbf{F_w} \\ \mathbf{F_{nw}} \end{pmatrix} = \begin{pmatrix} \mathbf{K_{w1}} & \mathbf{K_{w2}} \\ \mathbf{K_{nw1}} & \mathbf{K_{nw2}} \end{pmatrix} \begin{pmatrix} \mathbf{u_w} \\ \mathbf{u_{nw}} \end{pmatrix} \tag{4}$$

where the block matrices $\mathbf{K_{w1}}, \mathbf{K_{w2}}, \mathbf{K_{nw1}}$ and $\mathbf{K_{nw2}}$ denote the tissue stiffness matrices. If the nodes of the tissue and joints of the needle match, we have $\mathbf{F_{w}}_{6\times1} = [F_{N1x}\; F_{N1y} \ldots\; F_{N3x}\; F_{N3y}]^T$, otherwise F_{Nix} and F_{Niy} forces can be written as functions of the $\mathbf{F_w}$ components. The above FEM equation, includes only tissue stiffness model. However, the results can be generalized to tissue models that include tissue viscosity and mass as well. Considering zero force boundary condition, the external forces at the non-working nodes are all nulled, that is $\mathbf{F_{nw}} = \mathbf{0}$. In this case the working node interaction forces can be linearly expressed in terms of the working node displacements according to $\mathbf{F_w} = [\mathbf{K_{w1}} - \mathbf{K_{w2}}\mathbf{K_{nw2}^{-1}}\mathbf{K_{nw1}}]\mathbf{u_w}$. As a result, the interaction forces F_{Nix} and F_{Niy} are linear functions of the displacements of the working nodes which in turn are *nonlinear* functions of θ and α. The above derivations are valid for the stick mode, in which the needle is not cutting the tissue. For the slip mode, in which the tissue is being cut, FEM forces along needle link directions are set to zero and only the friction forces are applied. The net amount of force at each node can be decomposed into parallel and perpendicular components in order to determine an effective stiffness at each node.

The tissue-needle dynamics (2)-(3) can be presented in the state-space form

$$\begin{cases} \dot{x}_1 &= x_3 \\ \dot{x}_2 &= x_4 \\ \dot{x}_3 &= \frac{1}{3m}[F_{in} - \sum_{i=1}^{3} F_{Niy} - B_f x_3] \\ \dot{x}_4 &= -\frac{L\sum_{i=1}^{3} iF_{Nix}}{14mL^2+3I} + \frac{\tau_{in}}{14mL^2+3I} \end{cases} \tag{5}$$

where $x_1 = \alpha$, $x_2 = \theta$, $x_3 = \dot{\alpha}$ and $x_4 = \dot{\theta}$ are the states of the system. The nonlinear state-space equations in (5) can be re-written in the following general standard form for nonlinear systems suitable for the analysis of controllability

$$\dot{\mathbf{X}} = \mathbf{f}(\mathbf{X}) + \mathbf{g_1}u_1 + \mathbf{g_2}u_2, \tag{6}$$

where $\mathbf{X} = [x_1 \;\; x_2 \;\; x_3 \;\; x_4]^T$ is the vector of system states,

$u_1 = F_{in}$, $u_2 = \tau_{in}$, and

$$\mathbf{f}(\mathbf{X}) = \begin{pmatrix} x_3 \\ x_4 \\ -\frac{1}{3m}(\sum_{i=1}^{3} F_{Niy} + B_f x_3) \\ -\frac{L}{14mL^2+3I}\sum_{i=1}^{3} iF_{Nix} \end{pmatrix} \quad (7)$$

$$\mathbf{g_1} = \begin{pmatrix} 0 \\ 0 \\ \frac{1}{3m} \\ 0 \end{pmatrix}, \mathbf{g_2} = \begin{pmatrix} 0 \\ 0 \\ 0 \\ \frac{1}{14mL^2+3I} \end{pmatrix}. \quad (8)$$

B. Controllability of Rigid Needle Insertion

Controllability of a nonlinear system refers to the property of the system by which suitable input can be found such that the states of the system can reach any point within the state space from any initial condition in finite time. For the tissue-needle nonlinear dynamic system (6), controllability determines whether one can steer the needle-tip to any desired position at any desired velocity from any initial position and velocity; in other words, whether the user has full control over the position profile of the needle-tip. To investigate the controllability of the nonlinear system (6), one should check for the rank of the controllability matrix, defined as the matrix containing columns chosen from the following distribution [18]

$$\text{span}\{\mathbf{f}, \mathbf{g_1}, \mathbf{g_2}, [ad^k_{\mathbf{f}}, \mathbf{g_1}], [ad^k_{\mathbf{f}}, \mathbf{g_2}], [ad^k_{\mathbf{g_1}}, \mathbf{g_2}]\} \quad (9)$$

for $k = 1, 2, 3, \ldots$. Here, $[ad^1_{\mathbf{f}(\mathbf{X})}, \mathbf{g}] = [\mathbf{f}(\mathbf{X}), \mathbf{g}] := \frac{\partial \mathbf{g}}{\partial \mathbf{X}}\mathbf{f} - \frac{\partial \mathbf{f}}{\partial \mathbf{X}}\mathbf{g}$ is the *adjoint* or the *Lie bracket* of the two vectors $\mathbf{f}(\mathbf{X})$ and $\mathbf{g}$, and $[ad^k_{\mathbf{f}(\mathbf{X})}, \mathbf{g}] = [\mathbf{f}(\mathbf{X}), ad^{k-1}_{\mathbf{f}(\mathbf{X})}]$. The maximum k is chosen such that the above-mentioned distribution becomes involutive, in other words no higher-order Lie brackets add to the rank of the span. If the defined controllability matrix is full rank for the entire state space, in our case rank=4, the nonlinear system is controllable.

Using (7-8) we can derive the controllability matrix

$$\mathbf{\Psi} = \begin{pmatrix} \mathbf{g_1} & \mathbf{g_2} & [\mathbf{f}(\mathbf{X}), \mathbf{g_1}] & [\mathbf{f}(\mathbf{X}), \mathbf{g_2}] \end{pmatrix} \quad (10)$$

with $k = 1$, which includes columns two to five of the distribution (9). Since $\mathbf{g_1}$ and $\mathbf{g_2}$ are constant vectors, $[\mathbf{f}(\mathbf{X}), \mathbf{g_1}] = \frac{\partial \mathbf{f}}{\partial \mathbf{X}}\mathbf{g_1}$ and $[\mathbf{f}(\mathbf{X}), \mathbf{g_2}] = \frac{\partial \mathbf{f}}{\partial \mathbf{X}}\mathbf{g_2}$. Despite involving nonlinear functions, since F_{Nix} and F_{Niy} are functions of only $x_1 = \alpha$ and $x_2 = \theta$, we have

$$\frac{\partial \mathbf{f}}{\partial \mathbf{X}}\mathbf{g_1} = \begin{pmatrix} \frac{1}{3m} \\ 0 \\ -\frac{B_f}{9m^2} \\ 0 \end{pmatrix}, \frac{\partial \mathbf{f}}{\partial \mathbf{X}}\mathbf{g_2} = \begin{pmatrix} 0 \\ \frac{1}{14mL^2+3I} \\ 0 \\ 0 \end{pmatrix}, \quad (11)$$

and, as a result,

$$\mathbf{\Psi} = \begin{pmatrix} 0 & 0 & \frac{1}{3m} & 0 \\ 0 & 0 & 0 & \frac{1}{14mL^2+3I} \\ \frac{1}{3m} & 0 & -\frac{B_f}{9m^2} & 0 \\ 0 & \frac{1}{14mL^2+3I} & 0 & 0 \end{pmatrix}. \quad (12)$$

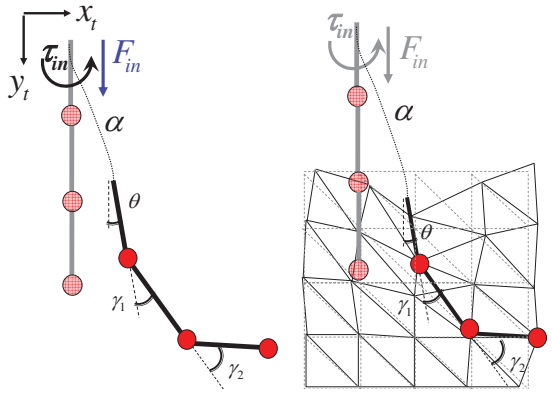

Fig. 2. General model of a flexible needle inside an FEM tissue.

Performing column-wise operations on columns 1 and 3, it is easily possible to show that matrix $\mathbf{\Psi}$ is full rank and the nonlinear system (6) is controllable. Therefore, the states of the system $x_1 = \alpha$, $x_2 = \theta$, $x_3 = \dot{\alpha}$ and $x_4 = \dot{\theta}$ and hence the output of the system can be controlled to any desired values using a suitable nonlinear feedback control. From a medical perspective, this means that using accurate manipulation of the needle base, either by the surgeon or a controlled robot, the needle tip can reach any desired point inside the tissue, in spite of possible tissue deformation. The controllability of the above system can also be intuitively justified, as the coupled system of the rigid needle and the soft tissue has two modes (α and θ) and the same number of control inputs. Considerations should be taken in the control of rigid needle inside a soft tissue regarding tissue damage. In the next section, we study effect of needle flexibility on system controllability.

III. Control of Flexible Needles in Soft Tissue

A. Dynamic model of flexible needles

In this section, in order to model the dynamics of flexible needles in the plane, we take the same approach as in [15] for angular springs model of flexible needles by considering two pseudo joints along the needle and the mass of each link at its distal end (as described for rigid needles in Section II). As shown in Figure 2, the unactuated pseudo joints are modeled by torsional springs which allows the needle model to conform to the bending shape of a flexible needle. Here we consider k_{b1} and k_{b2} as the stiffness of the pseudo joints and γ_1 and γ_2 as the joint angles. For the rigid needle in Section II, springs are infinitely stiff, resulting in zero joint angles. A more accurate model of the needle can be obtained at the cost of higher dynamic complexity by increasing the number of pseudo joints along the needle.

After deriving the kinetic energy of the needle, the potential energy of the pseudo joints due to needle flexibility, the interaction forces of the needle with the tissue, and the dissipative energy due to needle-tissue friction, the dynamic

model of the tissue-needle system can be written as[1]

$$\mathbf{M}\ddot{\mathbf{\Theta}} + \mathbf{C}\dot{\mathbf{\Theta}} + \mathbf{K}\mathbf{\Theta} = \mathbf{F} - \mathbf{G} - \mathbf{F}_f. \tag{13}$$

where, $\mathbf{\Theta} = [\alpha\ \theta\ \gamma_1\ \gamma_2]^T$ is the vector of generalized coordinates, $\mathbf{F} = [F_{in}\ \tau_{in}\ 0\ 0]^T$ is the vector of generalized input forces, and $\mathbf{F}_f = [-B_f\dot{\alpha}\ 0\ 0\ 0]^T$ represents the friction applied in the direction of needle movement. The friction vector $\mathbf{F}_f$ can also include viscous friction at the pseudo joints. The vector $\mathbf{G}$ represents the generalized forces applied to the joints, which are the forces of interaction between the tissue and the needle experienced at the three nodes converted from Cartesian coordinates attached to the needle to the joint space via the needle Jacobian. The counterpart for this vector in the rigid-needle dynamic equations (2)-(3) is $[\sum_{i=1}^{3} F_{Niy}\ \ L\sum_{i=1}^{3} iF_{Nix}]^T$. Similarly to the rigid case, F_{Nix} and F_{Niy} are linear functions of the working nodes, but nonlinear functions of the states of the system.

The symmetric mass matrix $\mathbf{M}_{4\times4}$ with components $\mathbf{M}_{ij}(\mathbf{\Theta}),\ i,j = 1,2,3,4$ is a nonlinear function of the generalized coordinates $\mathbf{\Theta}$, whereas the Coriolis and centrifugal matrix $\mathbf{C}_{4\times4}$ with components $\mathbf{C}_{ij}(\mathbf{\Theta}, \dot{\mathbf{\Theta}})$, is a nonlinear function of the generalized coordinates $\mathbf{\Theta}$ and $\dot{\mathbf{\Theta}}$ [2]. The matrix $\mathbf{K}$ is the diagonal stiffness matrix

$$\mathbf{K} = \begin{pmatrix} 0 & 0 & 0 & 0 \\ 0 & 0 & 0 & 0 \\ 0 & 0 & k_{b1} & 0 \\ 0 & 0 & 0 & k_{b2} \end{pmatrix}, \tag{14}$$

representing the spring effect at the joints.

Defining $\mathbf{X} := [x_1\ x_2\ \cdots x_8]^T = [\alpha\ \theta\ \gamma_1\ \gamma_2\ \dot{\alpha}\ \dot{\theta}\ \dot{\gamma}_1\ \dot{\gamma}_2]^T$ as the vector of system states, and $\mathbf{x_1} = [x_1\ x_2\ x_3\ x_4]^T$, the needle-tissue dynamics can be written in the general state-space form (6) as follows

$$\begin{cases} \dot{\mathbf{x}}_\mathbf{1} &= \mathbf{x_2} \\ \dot{\mathbf{x}}_\mathbf{2} &= \mathbf{h}(\mathbf{x_1}, \mathbf{x_2}) + \bar{\mathbf{g}}_1 u_1 + \bar{\mathbf{g}}_2 u_2 \end{cases} \tag{15}$$

with $\mathbf{f}(\mathbf{X}) = [\mathbf{x_2}\ \mathbf{h}(\mathbf{x_1}, \mathbf{x_2})]^T$, $\mathbf{g}_1 = [\mathbf{0}\ \bar{\mathbf{g}}_1]^T$, $\mathbf{g}_2 = [\mathbf{0}\ \bar{\mathbf{g}}_2]^T$,

$$\mathbf{h} = \begin{pmatrix} \sum_{k=1}^{4} \mathbf{M}_{1k}^{-1}(-\mathbf{C}\dot{\mathbf{\Theta}}_{\{k\}} - \mathbf{K}\mathbf{\Theta}_{\{k\}} + \mathbf{G}_{\{k\}} - \mathbf{F}_{f_{\{k\}}}) \\ \sum_{k=1}^{4} \mathbf{M}_{2k}^{-1}(-\mathbf{C}\dot{\mathbf{\Theta}}_{\{k\}} - \mathbf{K}\mathbf{\Theta}_{\{k\}} + \mathbf{G}_{\{k\}} - \mathbf{F}_{f_{\{k\}}}) \\ \sum_{k=1}^{4} \mathbf{M}_{3k}^{-1}(-\mathbf{C}\dot{\mathbf{\Theta}}_{\{k\}} - \mathbf{K}\mathbf{\Theta}_{\{k\}} + \mathbf{G}_{\{k\}} - \mathbf{F}_{f_{\{k\}}}) \\ \sum_{k=1}^{4} \mathbf{M}_{4k}^{-1}(-\mathbf{C}\dot{\mathbf{\Theta}}_{\{k\}} - \mathbf{K}\mathbf{\Theta}_{\{k\}} + \mathbf{G}_{\{k\}} - \mathbf{F}_{f_{\{k\}}}) \end{pmatrix}, \tag{16}$$

and

$$\bar{\mathbf{g}}_\mathbf{1}(\mathbf{x_1}) = \begin{pmatrix} \mathbf{M}_{14}^{-1} \\ \mathbf{M}_{24}^{-1} \\ \mathbf{M}_{34}^{-1} \\ \mathbf{M}_{44}^{-1} \end{pmatrix}, \qquad \bar{\mathbf{g}}_\mathbf{2}(\mathbf{x_1}) = \begin{pmatrix} \mathbf{M}_{13}^{-1} \\ \mathbf{M}_{23}^{-1} \\ \mathbf{M}_{33}^{-1} \\ \mathbf{M}_{43}^{-1} \end{pmatrix}. \tag{17}$$

[1]Due to space limitation, the derivation details are omitted.

[2]Due to lack of space and complexity of M and C, the details of these matrices are not provided in this paper.

Here the subscript $\{k\}$ denotes the kth element of the corresponding vector and $\mathbf{M}_{ij}^{-1}$ represents the element (i,j) of the inverse mass matrix $\mathbf{M}^{-1}$.

B. Controllability of Flexible Needle Insertion

Although it is possible to find a closed-form representation for $\mathbf{h}(\mathbf{x_1}, \mathbf{x_2})$, $\bar{\mathbf{g}}_\mathbf{1}(\mathbf{x_1})$ and $\bar{\mathbf{g}}_\mathbf{2}(\mathbf{x_1})$, deriving a closed-form expression for the nonlinear controllability matrix of such a model, as described in Section II-B, is cumbersome if not impossible. This is due to the fact that the controllability matrix requires differentiation of very complex functions up to the order m, for which the distribution achieved from the span of the set described in (9) becomes involutive. In order to analyze the controllability matrix for our case, we require at least 8 columns and thus, the Lie brackets of at least order $k = 2$. Although it might be possible to evaluate such a matrix numerically for a pre-planned task, the problem of solving for the controllability matrix for the entire space is not practical.

Nevertheless, assuming small deformations caused by needle flexibility, we can study the controllability of the linearized model of the flexible system around the operating point $\mathbf{X_0} = [\mathbf{x_{10}}^T\ \mathbf{x_{20}}^T]^T = [\alpha_0\ \theta_0\ 0\ 0\ \dot{\alpha}_0\ \dot{\theta}_0\ 0\ 0]^T$. Considering $\delta\mathbf{x_1}$, $\delta\mathbf{x_2}$ as linear deflections from the system operational states due to the small inputs δu_1 and δu_2, the nonlinear dynamics are linearized as follows

$$\begin{cases} \delta\dot{\mathbf{x}}_\mathbf{1} &= \delta\mathbf{x_2} \\ \delta\dot{\mathbf{x}}_\mathbf{2} &= \Phi_1\delta\mathbf{x_1} + \Phi_2\delta\mathbf{x_2} + \bar{\mathbf{g}}_1\delta u_1 + \bar{\mathbf{g}}_2\delta u_2 \end{cases} \tag{18}$$

where

$$\Phi_1 = \frac{\partial\mathbf{h}(\mathbf{x_1}, \mathbf{x_2})}{\partial\mathbf{x_1}}|_{\mathbf{x_0}} + \frac{\partial\bar{\mathbf{g}}_1(\mathbf{x_1})}{\partial\mathbf{x_1}}u_1|_{\mathbf{x_0}} + \frac{\partial\bar{\mathbf{g}}_2(\mathbf{x_1})}{\partial\mathbf{x_1}}u_2|_{\mathbf{x_0}}$$
$$\Phi_2 = \frac{\partial\mathbf{h}(\mathbf{x_1}, \mathbf{x_2})}{\partial\mathbf{x_2}}|_{\mathbf{x_0}}. \tag{19}$$

The partial derivatives of $\mathbf{h}(\mathbf{x_1}, \mathbf{x_2})$, $\bar{\mathbf{g}}_\mathbf{1}(\mathbf{x_1})$ and $\bar{\mathbf{g}}_\mathbf{2}(\mathbf{x_1})$ and hence Φ_1 and Φ_2 can be found from their closed-form expressions using the Symbolic Toolbox of MATLAB. Therefore, the system and input matrices related to the state-space form of the system can be derived from (18) and (19) as

$$\mathbf{A} = \begin{pmatrix} \mathbf{0_{4\times4}} & \mathbf{I}_4 \\ \Phi_1 & \Phi_2 \end{pmatrix}, \mathbf{B} = \begin{pmatrix} \mathbf{0_{4\times1}} & \mathbf{0_{4\times1}} \\ \bar{\mathbf{g}}_1|_{\mathbf{x_0}} & \bar{\mathbf{g}}_2|_{\mathbf{x_0}} \end{pmatrix}, \tag{20}$$

where $\mathbf{I}_4$ is the identity matrix of order four, $\mathbf{A}$ is the 8×8 system matrix and $\mathbf{B}$ is the 8×2 input matrix. Analysis of the linearized system shows that, regardless of the operational point at which the system is linearized, the system has at least *two* eigenvalues at zero. This can be interpreted as the integral action of the system for the α and θ modes, meaning that increasing the input signal for any of the modes, *i.e.* F_{in} or τ_{in}, causes continuous increase of these modes, which is an intuitive conclusion.

To investigate the controllability of the linearized system, we need check whether the controllability matrix [18]

$$\mathbb{C}_{8\times16} = [\mathbf{B} \mid \mathbf{AB} \mid \mathbf{A}^2\mathbf{B} \mid \ \ldots\ \mid \mathbf{A}^7\mathbf{B}]. \tag{21}$$

is full rank. Considering the rigid needle case in which α and θ were controllable, we effectively study whether we can control the states related to the introduced flexibilities. In order to test system controllability, we numerically evaluated the $\mathbb{C}$ matrix at different operational points around $[2\,cm\ \ \pi/4\,rad\ \ 0\ \ 0\ \ 0.2\,cm/s\ \ 0.04\,rad/s\ \ 0\ \ 0]$, while one parameter deviates at a time, with tissue effective stiffness $10\,kN/m$ along the direction and perpendicular to the needle, and needle joint stiffness $k_b = 5,000\,\mu Nm$ (based on the values reported in [15]). The numerical evaluation of the rank of the controllability matrix using MATLAB function *rank*[3], showed that the controllability matrix of the linearized model of the tissue-needle system is rank deficient (rank($\mathbb{C}$) < 8) in the majority of the points, with the condition number in the orders of 10^{13} to 10^{16}. Similar results are achieved for different operational points. This shows that the linearized model of such a flexible needle is locally uncontrollable, and thus, the needle-tip cannot be guaranteed to reach any desired configuration inside soft tissue. This, in fact, does not mean that the flexible needle cannot be steered to a predefined target as carried out in many clinical practice with success [4], [6], [19]. This is likely due to the fact that clinical applications may not necessarily require controlling all needle states presented here. This will be further examined in future work.

Note that although the linearized system is not controllable, the lack of controllability of the nonlinear system does not follow [18]. In a study of controllability of flexible-link manipulator for free space motions [20], it has been mentioned that one or more of the flexible modes are not controllable in certain configurations, called inaccessible positions. This is related to the fact that a flexible-link in free motion is under-actuated. However, the problem of flexible needle insertion in soft tissue is different as the tissue-needle interaction forces, affecting the pseudo joints, are functions of the controllable system states α and θ. Further studies are required for nonlinear controllability of such systems.

IV. Conclusions

In order to fully control the motion of a rigid or a flexible needle body and its tip inside a soft tissue via feedback control, we need to first determine whether such a needle-tissue system is controllable. We have shown that a rigid needle moving in a planar soft tissue modeled by FEM is dynamically controllable. As such, the needle-tip as a function of the system states, can theoretically reach any target position. To analyze controllability of the tissue-needle system for a flexible needle, we utilized a mass-spring model, based on the angular spring model of the needle [15], consisting a series of cascading masses and springs. Due to the complexity of the nonlinear dynamics of the coupled needle-tissue system and the need for second and higher order partial derivatives of these nonlinear functions, the analysis of controllability was carried out on a linearized model. This has shown that the flexible needle inside soft tissue is not locally full-state controllable. As a result, regular state-feedback controls cannot guarantee the needle to reach any desired configuration. Future work will aim towards the analysis of controllability for other models of flexible needles and designing suitable control systems for rigid and flexible needles.

[3]The rank is evaluated by the number of singular values of $\mathbb{C}$ that are larger than a tolerance number, which is determined by the size of the matrix and the floating point precision of maximum singular value of $\mathbb{C}$.

V. Acknowledgments

This work was supported in part by Natural Sciences and Research Engineering Council of Canada (NSERC) and Queen's University Advisory Research Committee (ARC).

References

[1] G. Fichtinger, T. DeWeese, and A. Patriciu et. al., "System for robotically assisted prostate biopsy and therapy with intraoperative CT guidance," *Acad Radiol*, vol. 9, no. 1, pp. 60–74, 2002.

[2] R. Alterovitz, J. Pouliot, R. Taschereau, I. Hsu, and K. Goldberg, "Simulating needle insertion and radioactive seed implantation for prostate brachytherapy," *Stud. in Health Tech. and Informat.*, pp. 19–25, 2003.

[3] N. Abolhassani, R. Patel, and M. Moallem, "Needle insertion into soft tissue: A survey," *Med. Eng. and Phys.*, vol. 29, no. 4, pp. 413–431, 2007.

[4] R. Alterovitz, K. Goldberg, and A. Okamura, "Planning for steerable bevel-tip needle insertion through 2d soft tissue with obstacles," in *Proc. of ICRA*, 2005, pp. 1640–1645.

[5] S. E. Salcudean, D. French, S. Bachmann, and R. Zahiri-Azar, "Viscoelasticity modeling of the prostate region using vibro-elastography," in *Proc. of MICCAI*, 2006, pp. 389–396.

[6] D. Glozman and M. Shoham, "Flexible needle steering and optimal trajectory planning for percutaneous therapies," in *Proc. of MICCAI*, 2004, pp. 137–144.

[7] N. Abolhassani, R. Patel, and F. Ayazi, "Minimization of needle deflection in robot-assisted percutaneous therapy," *Int. J. of Med. Robot. and Comp. Assis. Surg.*, vol. 3, no. 2, pp. 140–148, 2007.

[8] S. Misra, K. Reed, A. Douglas, K. Ramesh, and A. Okamura, "Needle-tissue interaction forces for bevel-tip steerable needles," in *Proc. IEEE Int. Conf. on Biomed. Rob. and Biomechat.*, 2008, pp. 224–231.

[9] S. P. DiMaio and S. E. Salcudean, "Needle insertion modeling and simulation," *IEEE Trans. on Rob. and Auto.*, vol. 19, no. 5, pp. 864–875, 2003.

[10] C. Duriez, C. Guébert, M. Marchal, S. Cotin, and L. Grisoni, "Interactive simulation of flexible needle insertions based on constraint models," in *Proc. of MICCAI*, 2009, pp. 291–299.

[11] S. P. DiMaio and S. E. Salcudean, "Needle steering and model-based trajectory planning," in *Proc. of MICCAI*, 2003, pp. 33–40.

[12] V. Duindam, R. Alterovitz, S. Sastry, and K. Goldberg, "Screw-based motion planning for bevel-tip flexible needles in 3d environments with obstacles," *Proc. of ICRA*, pp. 2483–2488, 2008.

[13] K. Hauser, R. Alterovitz, N. Chentanez, A. Okamura, and K. Goldberg, "Feedback control for steering needles through 3D deformable tissue using helical paths," *Proc. of Rob.: Sci. and Sys.*, 2009.

[14] K. Reed, A. Okamura, and N. Cowan, "Modeling and control of needles with torsional friction," *IEEE Trans. on Biomed. Eng.*, vol. 56, no. 12, pp. 2905–2916, 2009.

[15] O. Goksel, E. Dehghan, and S. E. Salcudean, "Modeling and simulation of flexible needles," *Med. Eng. and Phys.*, pp. 1069–1078, 2009.

[16] G. Hastings and W. Book, "Verification of a linear dynamic model for flexible robotic manipulators," in *Proc. of ICRA*, 1986, pp. 1024–1029.

[17] S. P. DiMaio and S. E. Salcudean, "Interactive simulation of needle insertion models," *IEEE Trans. on Biomed. Eng.*, vol. 52, no. 7, pp. 1167–1179, 2005.

[18] S. Sastry, *Nonlinear systems: analysis, stability, and control*. Springer Verlag, 1999.

[19] C. Wedlake, J. Moore, M. Rachinsky, D. Bainbridge, A. Wiles, and T. Peters, "Augmented reality guidance system for peripheral nerve blocks," in *Proc. of SPIE*, vol. 7625, 2010, p. 762537.

[20] S. Tosunoglu, S. Lin, and D. Tesar, "Accessibility and controllability of flexible robotic manipulators," *J. of Dyn. Sys., Meas., and Cont.*, vol. 114, pp. 50–58, 1992.